DTU Library

Fluid scaling laws of idealized wind farm simulations

van der Laan, M.P.; Andersen, S.J.; Kelly, M.; Baungaard, M.C.

[Link back to DTU Orbit](#)

Fluid scaling laws of idealized wind farm simulations

View the article online for updates and enhancements.
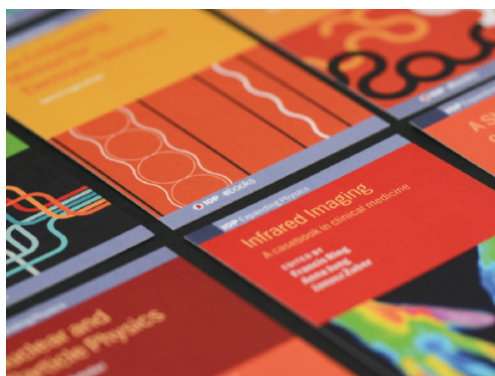
Fluid scaling laws of idealized wind farm simulations

M.P. van der Laan[1], S.J. Andersen[2], M. Kelly[1] and M.C. Baungaard[1]

[1]Technical University of Denmark, DTU Wind Energy, Risø Campus, DK-4000 Roskilde, Denmark

[2]Technical University of Denmark, DTU Wind Energy, Lyngby Campus, DK-2800 Kgs. Lyngby, Denmark

E-mail: `plaa@dtu.dk`

Abstract. Utilizing fluid scaling laws of idealized wind farm and wind resource simulations can reduce the computational effort and increase the understanding of the corresponding numerical model. However, not all fluid scaling laws are fully appreciated in the wind energy community. In this work, we employ dimensional analysis and Reynolds-averaged Navier-Stokes simulations of interacting wind turbine wakes and a Gaussian hill, and large-eddy simulations of a single wind turbine, to show that idealized wind farm simulations including terrain, subjected to a non-neutral atmospheric surface layer following Monin-Obukhov Similarity Theory, are independent of the inflow wind speed and wind turbine size due to Reynolds number similarity.

1. Introduction

Understanding the flow in and around wind farms is key to the development and improvement of numerical models that support reduction of levelized cost of wind energy. Wind turbines operate in atmospheric conditions that are characterized by high Reynolds numbers (Re) ranging from 10^6 up to 10^8 (based on the rotor diameter). Numerical simulations of a wind turbine wake can be made to be independent of Re, using an idealized atmospheric inflow representing the atmospheric surface layer (ASL). Here, an *idealized* ASL corresponds to an *implementation* of Monin-Obukhov Similarity Theory (MOST), whereby effects of atmospheric stability are *parameterized* via analytical expressions of properly normalized wind speed gradient (i.e., Re-independent). For a given stability state, the turbulence length scale implied by MOST does not depend on the wind speed[1], and therefore the velocity deficit and wake turbulence intensity of a single wind turbine are independent of the inflow velocity scale (such as friction velocity or a reference wind speed taken at a reference height). The wind speed independence can be used to simplify and expedite calculations of the annual energy production of a wind farm using Reynolds-averaged Navier-Stokes (RANS) solvers [1]. The same principle can be applied to flow over complex terrain with an idealized inflow, when the speedup[2] is independent of the inflow velocity scale. In addition, the wind turbine size is not an independent parameter as long as the Obukhov length, roughness length, and terrain height are scaled by the wind turbine size.

---

[1] This effectively assumes that the Obukhov length L, which by definition depends upon u_*^{-3}, is *prescribed* instead of *diagnosed* from the simulated flow; the L applied in the RANS equations does not depend on u_* (nor U).

[2] The *speedup* is defined as a ratio of hill-perturbed speed to (inflow) speed over flat terrain at a given height above the surface.

Dimensional analysis and subsequent scaling laws are fundamental tools within fluid mechanics, e.g. applying the Buckingham Π theorem for parametric reduction in complex flow problems. However, we find that universal scaling laws are unappreciated in the wind energy community, based on scientific literature, peer review processes [1] and discussions. Thus we would like to show fluid scaling laws relevant to idealized wind farm simulations. Section 2 presents the non-dimensional governing equations and discusses conditions for applicability of scaling laws. A simulation methodology is given in Section 3; it is used in Section 4 to provide numerical proof of each scaling law, via parametric studies. A validation is not performed in this work because our goal is to show the fluid scaling laws applicable to idealized simulations, not the quantitative results.

2. Scaling of governing equations

The equations that describe the flow in wind farms are the incompressible Navier-Stokes equations for mass ($\partial u_i / \partial x_i = 0$), and for momentum:

$$\frac{\partial u_i}{\partial t} + u_j \frac{\partial u_i}{\partial x_j} = -\frac{1}{\rho}\frac{\partial p}{\partial x_i} + \nu \frac{\partial}{\partial x_j}\left(\frac{\partial u_i}{\partial x_j} + \frac{\partial u_j}{\partial x_i}\right) + \frac{f_i}{\rho}, \tag{1}$$

where x_i are Cartesian coordinates, t is the time, u_i are the velocity components, p is the pressure, ρ is the fluid density, ν is the kinematic molecular viscosity and f_i are external forces per unit of volume, which for wind farm applications could represent wind turbine, Coriolis and buoyancy forces. The Navier-Stokes momentum equations including the external force can be written in non-dimensional form using the non-dimensional variables $u_i' \equiv u_i/\mathcal{U}$, $p' \equiv p/(\rho\mathcal{U}^2)$, $f_i' \equiv f_i\mathcal{L}/(\rho\mathcal{U}^2)$, $x_i' \equiv x_i/\mathcal{L}$, $t' \equiv t/\mathcal{T}$, with $\mathcal{U}$, $\mathcal{L}$ and $\mathcal{T}$ as characteristic scales of velocity, length and time, respectively:

$$\frac{\mathcal{L}}{\mathcal{U}\mathcal{T}}\frac{\partial u_i'}{\partial t'} + u_j'\frac{\partial u_i'}{\partial x_j'} = -\frac{\partial p'}{\partial x_i'} + \frac{1}{\text{Re}}\frac{\partial}{\partial x_j'}\left(\frac{\partial u_i'}{\partial x_j'} + \frac{\partial u_j'}{\partial x_i'}\right) + f_i', \tag{2}$$

with $Re = \mathcal{U}\mathcal{L}/\nu$ as the well-known Reynolds number describing the ratio of the inertial to viscous forces. Re based on the rotor diameter of utility scale wind turbines is large, and one can neglect viscous effects if the modelled wind turbine forces do not include a viscous component; e.g., a source term representing the thrust force per unit of volume as $|f_T| \propto \frac{1}{2}C_T\rho\mathcal{U}^2/\mathcal{L}$, for constant C_T and neglecting viscous surface effects via a rough wall boundary condition. In fact, if all external forces f_i scale with $\rho\mathcal{U}^2/\mathcal{L}$, and the characteristic time scale $\mathcal{T}$ of the flow is equal to $\mathcal{L}/\mathcal{U}$, then the Navier-Stokes momentum equations in normalized form do not depend on the characteristic scales of velocity and length. In other words, if we apply such a system of equations to wind farm simulations, the non-dimensional solution is independent of wind speed and wind turbine size, as long as Re is large enough. This is an important concept, which we will show to be true for idealized wind farm simulations in Section 4. If Coriolis or buoyancy forces are included in f_i, then the Navier-Stokes momentum equations become dependent on $\mathcal{U}$ and $\mathcal{L}$, since the Coriolis force is linear in $\mathcal{U}$ and the buoyancy force scales with a temperature scale instead of $\mathcal{U}$. Note that the wind turbine thrust coefficient is typically dependent on $\mathcal{U}$, which makes a wind farm simulation dependent on the inflow wind speed. However, this dependency can be removed by a scaling the wind turbine controller with $\mathcal{U}$, as discussed in previous work [1] and in Section 3.1.

The RANS (momentum) equations in non-dimensional form, using the Boussinesq (linear) stress-strain relation for the Reynolds-stress, can be written as:

$$U_j'\frac{\partial U_i'}{\partial x_j'} = -\frac{\partial P'}{\partial x_i'} + \frac{\partial}{\partial x_j'}\left[\left(\frac{1}{\text{Re}} + \nu_T'\right)\left(\frac{\partial U_i'}{\partial x_j'} + \frac{\partial U_j'}{\partial x_i'}\right)\right] + F_i', \tag{3}$$

where $U_i' \equiv U_i/\mathcal{U}$, $P' \equiv P/(\rho\mathcal{U}^2)$ and $F_i' \equiv F_i\mathcal{L}/(\rho\mathcal{U}^2)$, with U_i, P' and F_i as Reynolds-averaged variables and P represents the modified pressure including the turbulent kinetic energy. In addition, $\nu_T' \equiv \nu_T/(\mathcal{U}\mathcal{L})$ is the normalized eddy-viscosity with ν_T as the dimensional eddy-viscosity. The normalized RANS equations are also independent of the characteristic velocity and length scales, if the same conditions apply as mentioned for the normalized Navier-Stokes momentum equations and ν_T scales with $\mathcal{U}\mathcal{L}$. In other words, the turbulence model should predict an eddy-viscosity that scales linearly with a characteristic turbulence scale of velocity, u_*, and length, ℓ; i.e., $\mathcal{U} \propto u_*$ and $\mathcal{L} \propto \ell$. For example, the k-ε turbulence model for atmospheric flows has this property since $\nu_T = C_\mu k^2/\varepsilon$, with C_μ as a constant, k as the turbulent kinetic energy and ε as the destruction of k, where k and ε scale with $\mathcal{U}^2$ and $\mathcal{U}^3/\mathcal{L}$, respectively. In the neutral atmospheric surface layer, the k-ε turbulence model would predict an eddy-viscosity that varies linearly with height: $\nu_T = u_*\ell = u_*\kappa z$, where u_* is the friction velocity, κ is the von Kármán constant and z is the height. A non-neutral surface layer following MOST predicts a non-linear eddy-viscosity $\nu_T = u_*\kappa z/\Phi_m$, where Φ_m represents the normalized stream-wise velocity gradient $\Phi_m \equiv \kappa z/u_* \, dU/dz$. Φ_m is a function of the Obukhov length L, which is a measure of the atmospheric stability. The non-linear eddy-viscosity following MOST does not violate the model independence of characteristic velocity and length scales because the magnitude of ν_T still scales with a single characteristic velocity and length scale, and the Φ_m function is not dependent on $\mathcal{U}$ and $\mathcal{L}$, it only introduces an additional length scale L. This may seem counter intuitive to the reader, and therefore, we will show that this statement is true by performing numerical simulations of wind turbines operating in non-neutral ASLs following MOST in Sections 4.1.1, 4.2 and 4.3.

It is also possible to model an eddy viscosity profile (and velocity profiles) that represent an idealized atmospheric boundary layer (ABL) using a limited length scale turbulence closure, where a finite boundary layer depth is modeled by a setting a maximum turbulence length scale, Coriolis forces are present and the flow is driven by setting a constant geostrophic wind speed [2]. This idealized ABL inflow profile, in non-dimensional form, is only dependent on two non-dimensional numbers, which can be written as two Rossby numbers [3]. However, both the magnitude and shape of the ABL profiles of the eddy viscosity and velocity are dependent on the characteristic velocity scale $\mathcal{U}$, i.e. $\nu_T \not\propto \mathcal{U}$ and $U \not\propto \mathcal{U}$, which means that this setup is not Re-independent.

3. Methodology

The numerical simulations are performed with EllipSys3D, the in-house finite volume flow solver of DTU Wind Energy, initially developed by Michelsen [4] and Sørensen [5]. In this work, we employ the RANS and LES models of EllipSys3D to test the Re-similarity of idealized wind farm simulations, as discussed in Section 2. Three test cases are simulated with the RANS model, a single wake, a double wake including wind turbine control and a Gaussian hill (without wind turbines), a schematic overview is given in Figure 1. The LES model is only used for the single wake case. The wind turbine model in the RANS simulations is based on the NREL-5MW reference wind turbine [6], which has a rotor diameter and hub height of $D = 126\,\mathrm{m}$ and $z_H = 90\,\mathrm{m}$, respectively. The inflow is defined by MOST and the wind direction is set to $270°$, hence the double wake case represents two wind turbines aligned with the inflow direction. A $5D$ inter spacing is used for the double wake case. For the single and double wake cases, the flow is extracted at a $5D$ downstream distance behind the most downstream wind turbine. The Gaussian hill represents an 2D axisymmetric Gaussian hill, where the height $h(r)$ is defined as:

$$h(r) = H\exp\left(-\frac{r^2}{2\sigma^2}\right), \quad \sigma = \frac{H\exp\left(-\frac{1}{2}\right)}{\tan\left(\alpha_{\max}\right)}, \tag{4}$$

where $r^2 = x^2 + y^2$, with x and y as the streamwise and lateral coordinates, respectively, σ is the radial standard deviation, H is the hill height and α_{max} is the maximum hill slope (located at $r = \pm\sigma$) set to 20°. The hill is placed at the center of the domain.
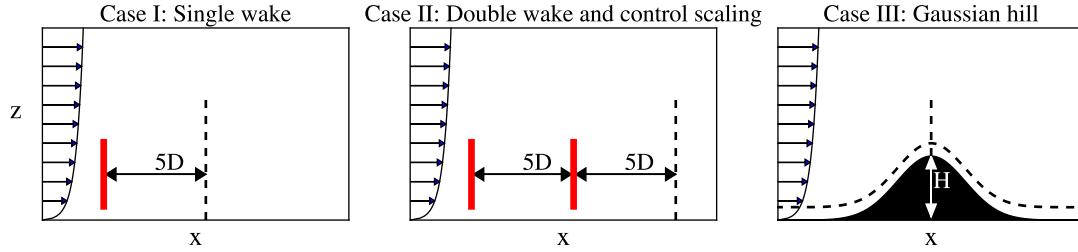

Figure 1. Schematic overview of test cases. Red filled rectangles represent the wind turbine rotor(s). Dashes lines represent the locations where the flow is extracted.

3.1. RANS

The turbulence in the RANS simulations is modeled by a two-equation k-ε model that is in balance with MOST inflow profiles. This is done by including conventional buoyant production/destruction (B) terms in each transport equation, with B parameterized in terms of normalized wind speed gradient for a given imposed stability (Obukhov length L). By using an additional source term in the k-equation and corresponding (height-dependent) $C_{\varepsilon,3}$ coefficient on B in the ε-equation, we avoid the necessity of a temperature equation and simulate flow consistent with MOST [7] (and without buoyancy sources in the momentum equations). In this work, the k-ε MOST model is also incorporated with a turbulence model developed for wind turbine wake simulations under neutral atmospheric conditions, which is known as the k-ε-f_P model [8]. Consistent implementation is accomplished by extending the definition of the f_P inflow shear parameter $\tilde{\sigma}$, to include stability:

$$\tilde{\sigma} = \frac{1}{\sqrt{C_\mu}} \sqrt{\frac{\Phi_m(\zeta)}{\Phi_\varepsilon(\zeta)}}, \tag{5}$$

where $C_\mu = 0.03$ is the eddy viscosity constant, $\zeta \equiv z/L$ with L the Obukhov length, and $\{\Phi_m, \Phi_\varepsilon\}$ are the MOST similarity functions for dimensionless wind shear and dissipation rate, respectively. The coupled k-ε turbulence model is in balance with any inflow following MOST, due to equation (5). It should be noted that the coupled model has not yet been validated for wind turbine wakes subjected to a non-neutral ASL, and may need re-calibration.

The wind turbine is represented by an Actuator Disk (AD) [9], using a generic formulation of the normal and tangential load distributions with root and tip corrections, as introduced by Sørensen et al. [10]. The generic AD model assumes constant circulation and compares surprisingly well with AD forces based on airfoil data (for both uniform and sheared inflow), and depends only on the thrust coefficient C_T and tip speed ratio λ. To ensure that total thrust, torque, and power output are consistent with the input C_T and C_P, we employ the generic AD model including additional scaling of the normal force distribution $\Delta F_{n,ij}$ with C_T, and scaling the tangential force distribution $\Delta F_{\theta,ij}$ with C_P and λ; the force distributions on each actuator

disk element i, j are thus implemented as:

$$\Delta F_{n,ij} = \frac{\frac{1}{2}\rho C_T A U_\infty^2 \Delta F_{n,ij}^0}{\sum_i \left(\sum_j \left[\Delta F_{n,ij}^0 \Delta A_{ij} \right] \right)}, \qquad \Delta F_{n,ij}^0 = 4\rho q_0 \frac{gF}{\chi_i} \left(\lambda \chi_i + \frac{1}{2} q_0 \frac{gF}{\chi_i} \right) \frac{U_{\mathrm{AD},ij}^2 \Delta A_{ij}}{\left(1 + \sqrt{1 - C_T} \right)^2},$$

$$\Delta F_{\theta,ij} = \frac{\frac{1}{2}\rho C_P A U_\infty^2 \Delta F_{\theta,ij}^0}{\lambda \sum_i \left(\chi_i \sum_j \left[\Delta F_{\theta,ij} \Delta A_{ij} \right] \right)}, \quad \Delta F_{\theta,ij}^0 = 2\rho q_0 \frac{gF}{\chi_i} \frac{U_{\mathrm{AD},ij}^2 \Delta A_{ij}}{1 + \sqrt{1 - C_T}}.$$

$$(6)$$

Here, the i and j indices represent the radial and azimuthal directions, respectively, χ_i is the local radius normalized by the rotor radius, ΔA_{ij} is the area of the AD element, $U_{\mathrm{AD},ij}$ is the local stream-wise velocity, U_∞ is the freestream velocity at hub height, and A is the total AD area. Furthermore, g and F are root and tip corrections, respectively, and q_0 is a dimensionless reference circulation; the full definitions of g, F and q_0 can be found in Sørensen et al. [10].

In addition to the scaling corrections above, we also extend the analytic AD model with a control method suited for wind farm simulations, where the 'freestream' velocity is unknown for any AD located in the wake of another AD. In previous work [11], a control method was developed based on fixed normalized force distributions, where C_T and C_P are replaced with C_T^* and C_P^*, which resemble thrust and power coefficients based on the streamwise velocity integrated over the AD $\langle U_{AD} \rangle$. Prior to a wind farm simulation, single AD simulations for every wind speed are run with known C_T, C_P and λ-curves (based on the NREL-5MW rotor [6]) to obtain relations for $C_T^*(\langle U_{AD} \rangle)$, $C_P^*(\langle U_{AD} \rangle)$, $\lambda(\langle U_{AD} \rangle)$ and $U_\infty(\langle U_{AD} \rangle)$. *Re*-similarity of the single AD simulations can be used to run the simulations consecutively by updating the C_T, C_P and λ for every new case, without updating the global inflow, which saves an order of magnitude in computational effort because only local changes need to be calculated [1]. We obtain the analytic AD model for wind farm simulations by substituting the relations $C_T = C_T^*(\langle U_{AD} \rangle / U_\infty)^2$ and $C_P = C_P^*(\langle U_{AD} \rangle / U_\infty)^3$ in eq. (6). Unlike the original AD force control method from previous work [11], the analytic AD model with control still depends on U_∞ as input, and therefore a relation between U_∞ and $\langle U_{AD} \rangle$ is required. Note that we could have chosen a different force distribution method, for example a AD based on airfoil data, without violating *Re*-similarity. This is because the force of an AD based on airfoil data scales with $\rho \mathcal{U}^2 / \mathcal{L}$, since the viscous blade forces are typically neglected, as discussed in Section 2.

As shown in previous work [1], the AD control can be made independent of the inflow wind speed U_∞ by multiplying $\langle U_{AD} \rangle$ in $C_T^*(\langle U_{AD} \rangle)$, $C_P^*(\langle U_{AD} \rangle)$, $\lambda(\langle U_{AD} \rangle)$ and $U_\infty(\langle U_{AD} \rangle)$ by a factor U_H / U_∞, where U_H is the desired wind speed to be simulated and U_∞ is the actual inflow wind speed. This method relies on the *Re*-similarity of interacting wind turbine wakes subjected to an inflow based on MOST, which is proven numerically in Section 4.2.

The numerical domain of the RANS simulations of Cases I and II consists of a Cartesian grid with a rough wall boundary condition at the bottom [12], symmetry conditions at the lateral boundaries and an inlet condition at the western and top boundaries, at which MOST profiles for U, k and ε are set. The area around the AD(s) uses a refined cell spacing of $D/8$, which is fine enough to capture the wake deficit [8]. The Gaussian hill simulation of Case III uses a curvilinear grid where the cell spacing around the hill is set to $H/8$. Details of the numerical setup are further discussed in previous work [8, 7], but they are not important for proving the fluid scaling laws, as long as the boundary conditions are consistent with MOST and all grid parameters scale by the rotor diameter or terrain height.

The shape of the MOST inflow profiles are defined by a turbulence intensity based on k, I_∞, and the stability (we use $\zeta = z_H / L$). Here the reference height z_H represents the wind turbine hub height. The magnitudes of the inflow profiles of U and k are, in effect, set by the friction

velocity. For a given ζ and I_∞, we can set the friction velocity u_* and roughness length z_0 as

$$u_* = U_\infty I_\infty \sqrt{3/2} C_\mu^{\frac{1}{4}} \Phi_\varepsilon (\zeta)^{-\frac{1}{4}} \Phi_m (\zeta)^{\frac{1}{4}}, \qquad z_0 = \frac{z_H}{\exp\left(\kappa U_\infty / u_* + \Psi_m (\zeta)\right) - 1}, \qquad (7)$$

where $\Phi_m (\zeta)$, $\Phi_\varepsilon (\zeta)$ and $\Psi_m (\zeta)$ are MOST similarity functions used in the k-ε model that is in balance with MOST [7].

3.2. LES

The turbulence in the LES is modelled using a subgrid-scale model by Deardorff [13], which applies a spatial filter to the Navier–Stokes equations. The turbulent structures larger than the spatial filter is resolved in both time and space, which means that scaling is also required in time. The wind turbine is modelled using the Actuator Line (AL) method as introduced by Sørensen and Shen [14], where body forces are introduced in the flow along rotating lines. The modelled turbine corresponds to a stiff NM80 [15] ($D = 80$ m) with a fixed rotational speed in order to also meet the time scaling by having a constant tip speed ratio. The body forces are derived from airfoil polars at a single Re of $3 \cdot 10^6$, and hence effectively Re-independent. The mesh is $20D \times 10D \times 10D$ in the streamwise, lateral, vertical directions, respectively. The grid is uniformly distributed in a central region with a constant grid spacing of $D/50$. Far field boundary conditions are applied on the sides as well as inlet and outlet boundary conditions. The turbine is positioned in $(x, y, z) = (8D, 5D, 5D)$. The inflow is uniform with turbulent fluctuations imposed $2.5D$ upstream of the turbine using body forces corresponding to a so-called Mann box, see [16], [17]. The Mann box has been generated using a turbulence length scale $L = D/2$, and $\Gamma = 3.0$, which describes the anisotropy of the generated turbulence, $\alpha\epsilon^{2/3} = 0.1$, where α is the spectral Kolmogorov constant, ϵ, is the specific rate of turbulent dissipation. Note, that the body forces have been scaled according to the free stream velocity U_∞ to get the same turbulence intensity in the inflow, see force coefficients in Table 1. A similar scaling of the turbulent fluctuations, where performed in Andersen et al. [18], although it should be noted that a normalized version of the flow solver was used as opposed to the present version in SI-units.

4. Results

The Re-similarity of the three test cases, as illustrated in Figure 1, is numerically proven in RANS using two neutral cases, $\zeta = 0$, with two ambient turbulence intensities, $I_\infty = 5\%$ and $I_\infty = 10\%$, a stable case, $\zeta = 0.5$, $I_\infty = 5\%$, and an unstable atmospheric inflow case, $\zeta = -0.5$, $I_\infty = 15\%$. Each atmospheric inflow case is simulated with two freestream wind speeds at hub height, $U_\infty = 1$ m/s and $U_\infty = 100$ m/s, and two size scaling factors s. For the AD cases (Cases I and II), $s = 1$ corresponds to an AD with a hub height and rotor diameter equal to the NREL-5MW reference wind turbine and $s = 2$ represents the same wind turbine with $D = 252$ m and $z_H = 180$ m. For the Gaussian hill (Case III), $s = 1$ represents a hill height and reference height of $H = 126$ m and $z_H = 90$ m, respectively, and for $s = 2$ both the hill height and reference height are multiplied by a factor 2 ($H = 252$ m and $z_H = 180$ m). The Re-similarity of the single wake case is also numerically proven with LES.

4.1. Case I: Single wake

4.1.1. RANS Figure 2 depicts the Re-similarity of streamwise velocity and turbulence intensity of a single AD (Case I from Figure 1) taken at a downstream distance of five rotor diameters. In addition, results of two thrust coefficients C_T are depicted in Fig. 2, while a fixed tip speed ratio of 7.5 and power coefficient of 0.5 are set. It is clear that both the inflow wind speed and wind turbine size do not influence the normalized streamwise velocity and turbulence intensity
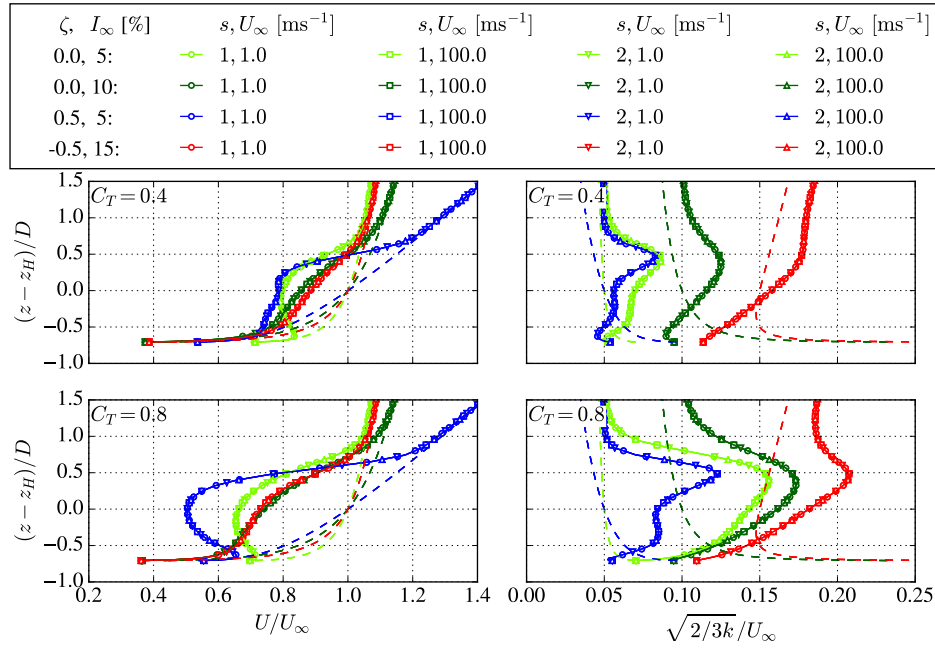
Figure 2. Case I: *Re*-similarity of a single wind turbine wake. Flow is extracted at downstream distance of $5D$, for different atmospheric conditions, thrust coefficients and inflow wind speeds and wind turbine sizes. Dashed lines represent the inflow profiles.

in the wake. The thrust coefficient is the main parameter that determines the wake. The effect of the tip speed ratio only changes the force distributions, not the magnitude, and the power coefficient influences the magnitude of the tangential force. Since both the force distributions and the tangential forces have a minor influence on the wake, as shown by Simisiroglou et al. [19] and Sørensen et al. [10], respectively, the tip speed ratio and the power coefficient are less important with respect to the thrust coefficient.

4.1.2. LES Three simulations have been performed to show how the fluid scaling also applies in dynamic simulations. The mean inflow velocity is modelled at 5, 10, and 20 m/s with different fixed rotational speeds in order to also meet the time scaling by having a constant tip speed ratio. Additionally, the inflow turbulence has been scaled relative to the inflow by C_{Mann}, so that the turbulence intensity is the same for all the three simulations.

Table 1. Overview of variables for LES.

U_∞ [m/s]	Ω [rad/s]	C_{Mann}	Δt [ms]	T [s]
5	1.2055	0.5	5	1680
10	2.4110	1.0	2.5	840
20	4.8220	2.0	1.25	420

Table 1 gives an overview of the parameters applied, i.e. free stream velocity U_∞, rotational speed Ω, the amplification factor imposed on the Mann turbulence C_M, time step, and the total simulated time. These parameters yield constant λ and C_T. Note, how the time scaling corresponds to using different time steps and simulating different lengths of time. Essentially, this means that the blades rotates approximately $1.5°$ for each time step and that the rotor operation and wake are compared during 230 rotor revolutions rather than *e.g.* 10 min average.

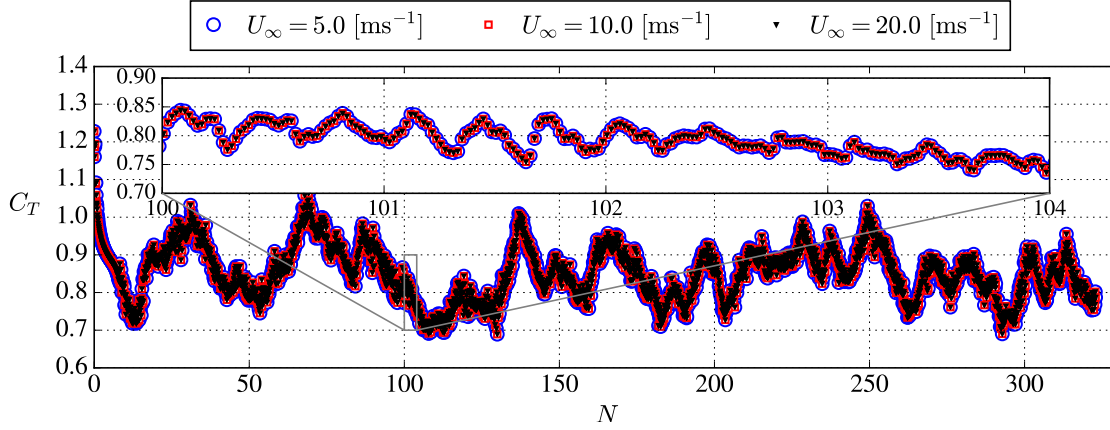The initial transient of 92 rotor revolutions has been discarded as the wake develops through the domain.

Figure 3. Case I: Instantaneous C_T versus time (as rotor revolutions, N) shown every $10\ \Delta t$.
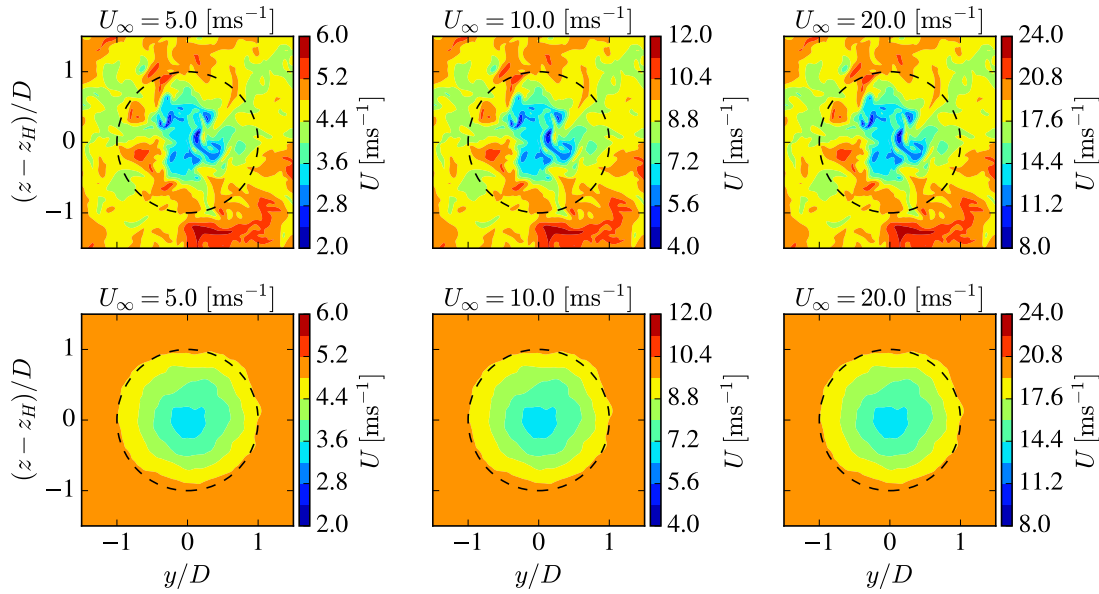

Figure 4. Case I: single turbine wake using AL in LES. Flow extracted $5D$ downstream of turbine, for different U; dashed circle shows turbine extent. Top: instantaneous contours of streamwise velocity after 283 rotor revolutions; bottom: velocity averaged over 230 revolutions.

Figure 3 depicts the instantaneous C_T for the three simulations as function of rotor revolutions N. It is clearly seen that C_T is identical for all simulations for each rotor revolution despite the turbulent inflow. Figure 4 shows an example of an instantaneous flow field extracted $5D$ downstream as well as the time averaged field for all three simulations. Both the instantaneous and averaged results are identical; the subgrid-scale model only has a spatial dependence when the simulations are scaled correctly with time.

4.2. Case II: Double wake and control scaling
Figure 5 illustrates the Re-independence of simulated flow around two in-line ADs, using AD control. Two cases are shown; one represents a case corresponding to hub-height inflow below

rated wind speed ($U_H = 8$ m/s), and the other above rated wind speed ($U_H = 12$ m/s). We remind that the inflow wind speed at hub height is also set to drastically different magnitudes, to demonstrate: 1 m/s and 100 m/s, with the AD wind speed controller then scaled to simulate a desired wind speed U_H, as discussed in Section 3.1. The wake deficit and turbulence intensity, shown at downstream distance of $5D$ behind the second AD is only dependent on the chosen flow case that set the AD controller, the ambient turbulence intensity and the atmospheric stability.
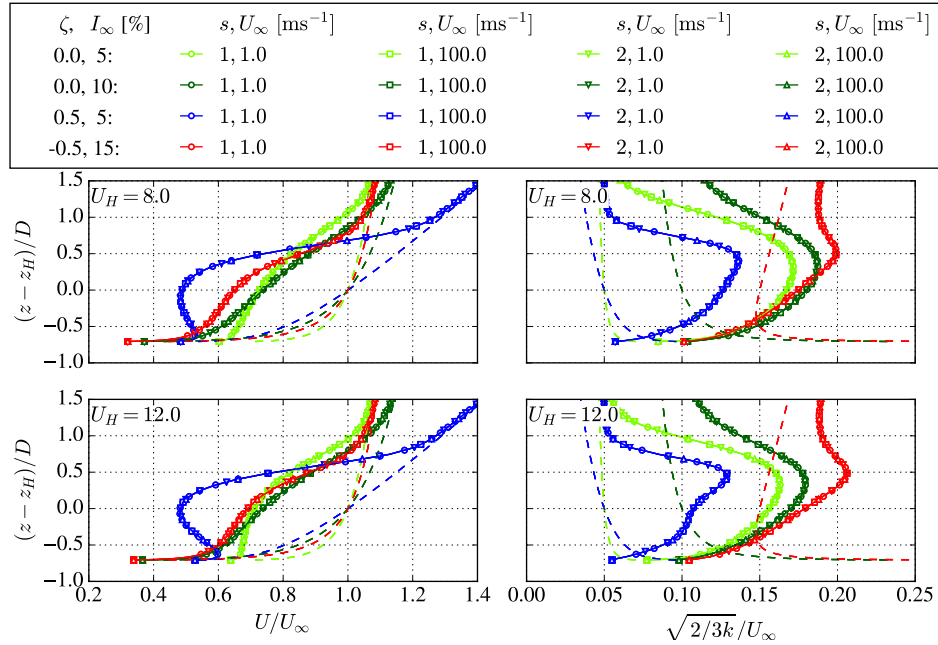

Figure 5. Case II: Re-similarity of a double wind turbine wake including AD controller. Flow is extracted at downstream distance of $5D$ behind the second wind turbine, for different atmospheric conditions, control scaling wind speeds U_H, inflow wind speeds and wind turbine sizes. Dashed lines represent inflow profiles.

4.3. Case III: Gaussian hill
Figure 6 shows the Re-similarity of both the speed-up and turbulence intensity, displaying the vertical profile of each over the hill top, as well as streamwise transects at height $H/5$ above ground. Re-independence can be exploited to find speed-ups under neutral conditions, from a single simulation per wind direction. From the results of the single and double wake cases from Sections 4.1.1 and 4.2 along with those from Figure 6, we can conclude: wind farm simulations in complex terrain, subjected to idealized atmospheric inflow following MOST, are independent of wind speed and rotor size due to the Re-similarity.

5. Conclusions
RANS simulations of a single wind turbine wake, a double wind turbine wake with force control, and a Gaussian hill in idealized atmospheric conditions defined by MOST, are employed to show that normalized streamwise velocity and turbulence intensity are independent of the inflow wind speed and wind turbine size, following Re-similarity. The simulated RANS fields are dependent on two inflow parameters—the ambient (inflow) turbulence intensity and prescribed stability— along with one wind turbine parameter, the thrust coefficient. In addition, three LES of a single wind turbine using actuator-line modelling, with different inflow wind speeds, confirm the
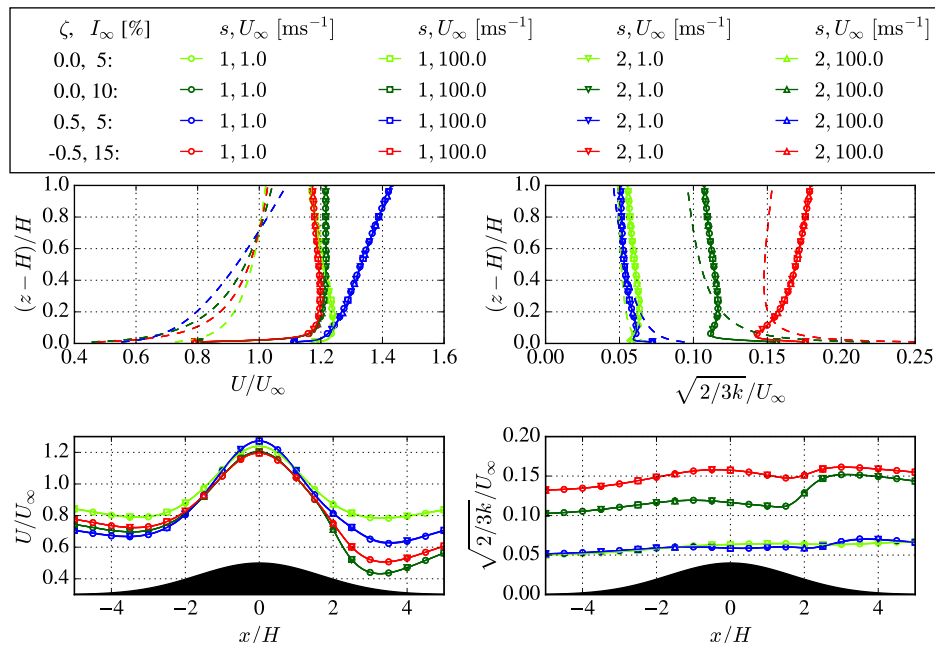
Figure 6. Case III: *Re*-similarity of flow over a Gaussian hill, for different atmospheric conditions, inflow wind speeds, and hill sizes. Top plots: profiles of speed-up and turbulence intensity extracted above hilltop; dashed lines represent inflow profiles. Bottom plots: speed-up and turbulence intensity extracted along streamwise center-line of hill, at $z = H/5$.

Re-similarity for both instantaneous and time-averaged streamwise velocity and wind turbine thrust force. *Re*-similarity can be exploited to reduce the number of simulations necessary to perform wind resource assessment and calculation of energy losses due to wake effects.

References

[1] van der Laan M P, Andersen S J and Réthoré P E 2019 *Wind Energy Science* **4** 645
[2] Apsley D D and Castro I P 1997 *Boundary-Layer Meteorology* **83** 75
[3] van der Laan M P, Kelly M, Floors R and Peña A 2019 *Wind Energy Science Discussions* **2019** 1
[4] Michelsen J A 1992 Basis3d - a platform for development of multiblock PDE solvers. Tech. rep. DTU
[5] Sørensen N N 1994 *General purpose flow solver applied to flow over hills* Ph.D. thesis DTU
[6] Jonkman J, Butterfield S, Musial W and Scott G 2009 Definition of a 5-MW Reference Wind Turbine for Offshore System Development Tech. rep. National Renewable Energy Laboratory
[7] van der Laan M P, Kelly M C and Sørensen N N 2017 *Wind Energy* **20** 479
[8] van der Laan M P, Sørensen N N, Réthoré P E, Mann J, Kelly M C, Troldborg N, Schepers J G and Machefaux E 2015 *Wind Energy* **18** 889
[9] Réthoré P E, van der Laan P, Troldborg N, Zahle F and Sørensen N N *Wind Energy* **17** 919
[10] Sørensen J N, Nilsson K, Ivanell S, Asmuth H and Mikkelsen R F 2020 *Renewable Energy* **147** 2259
[11] van der Laan M P, Sørensen N N, Réthoré P E, Mann J, Kelly M C and Troldborg N 2015 *Wind Energy* **18** 2223
[12] Sørensen N N, Bechmann A, Johansen J, Myllerup L, Botha P, Vinther S and Nielsen B S 2007 *Journal of Physics: Conference series* **75** 1
[13] Deardorff J W 1972 *Journal of the Atmospheric Sciences* **29** 91
[14] Sørensen J N and Shen W Z 2002 *Journal of Fluids Engineering* **124** 393
[15] Madsen H A *et al.* 2010 The DAN-AERO MW Experiments Tech. rep. DTU, Risø
[16] Mann J 1994 *Journal of Fluid Mechanics* **273** 141
[17] Mann J 1998 *Probabilistic engineering mechanics* **13** 269
[18] Andersen S J, Sørensen J N and Mikkelsen R F 2017 *Philosophical Transactions of the Royal Society A: Mathematical, Physical and Engineering Sciences* **375** 20160107–20160107 ISSN 14712962, 1364503x
[19] Simisiroglou N, Breton S P and Ivanell S 2017 *Wind Energy Science* **2** 587